Updated constraints on Z' and W' bosons decaying into bosonic and leptonic final states using the run 2 ATLAS data

P. Osland[*]

Department of Physics and Technology, University of Bergen, Postboks 7803, N-5020 Bergen, Norway

A. A. Pankov[†]

The Abdus Salam ICTP Affiliated Centre, Technical University of Gomel, 246746 Gomel, Belarus; Institute for Nuclear Problems, Belarusian State University, 220030 Minsk, Belarus, and Joint Institute for Nuclear Research, Dubna 141980, Russia

I. A. Serenkova[‡]

The Abdus Salam ICTP Affiliated Centre, Technical University of Gomel, 246746 Gomel, Belarus

(Received 8 January 2021; accepted 19 February 2021; published 29 March 2021)

The full ATLAS run 2 dataset with a time-integrated luminosity of 139 fb^{-1} in the diboson and dilepton channels is used to probe benchmark models with extended gauge sectors: the E_6-motivated grand unification models, the left-right symmetric model, and the sequential standard model [extended gauge model (EGM)]. These all predict neutral Z' vector bosons, decaying into lepton pairs $\ell\ell$ or into electroweak gauge boson pairs WW, where one W in turn decays semileptonically. The 95% C.L. exclusion limits on the Z' resonance production cross section times the branching ratio to electroweak gauge boson pairs and to lepton pairs in the mass range of ~1 to 6 TeV are converted to constraints on the Z-Z' mixing parameter and the heavy resonance mass. We present exclusion regions on the parameter space of the Z' which are significantly extended compared to those obtained from the previous analyses performed with LHC data collected at 7 and 8 TeV in run 1 as well as at 13 TeV in run 2 at a time-integrated luminosity of 36.1 fb^{-1} and are the most stringent bounds to date. Also presented, from a similar analysis of electrically charged W' bosons arising in the EGM, which can decay through $W' \to WZ$ and $W' \to \ell\nu$, are limits on the W-W' mixing parameter and the charged W' vector boson mass.

DOI: 10.1103/PhysRevD.103.053009

I. INTRODUCTION

One of the main goals of the physics program at the Large Hadron Collider (LHC) is to search for new resonant or nonresonant phenomena that become visible in high-energy proton-proton collisions. A prominent possible signature of such phenomena would be the production of a heavy resonance with its subsequent decay into a pair of leptons or into electroweak vector bosons. Many scenarios beyond the Standard Model (SM) predict such signals. Possible candidates are neutral and charged heavy gauge bosons which are commonly referred to as Z' and W' bosons, respectively [1]. Strong constraints have already been set on the production of such new heavy particles.

At the LHC, heavy Z' and W' bosons could be observed through their production as s-channel resonances with subsequent leptonic decays

$$pp \to Z'X \to \ell^+\ell^-X \tag{1}$$

and

$$pp \to W'X \to \ell\nu X, \tag{2}$$

respectively, where, in what follows, $\ell = e,\ \mu$ unless otherwise stated. The production of Z' and W' bosons at hadron colliders is expected to be dominated by the Drell-Yan (DY) mechanism, $q\bar{q}/q\bar{q}' \to Z'/W'$. The Feynman diagrams for the Z' (W') boson production at the parton level and their dilepton and diboson decays are illustrated in Fig. 1.

Leptonic final states provide a low-background and efficient experimental signature that results in excellent

[*]Per.Osland@uib.no
[†]pankov@ictp.it
[‡]Inna.Serenkova@cern.ch

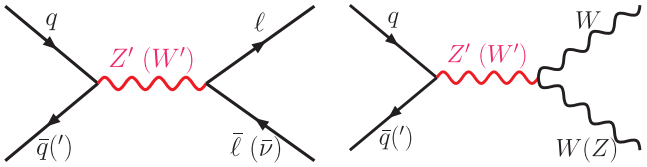

FIG. 1. Parton-level Feynman diagrams for Z' (W') production with dilepton and diboson decays.

sensitivity to new phenomena at the LHC. Specifically, these processes (1) and (2) offer the simplest event topology for the discovery of Z' and W' with a large production rate and a clean experimental signature. These channels offer the most promising discoveries at the LHC [2–7]. There have also been many theoretical studies of Z' and W' searches at the high-energy hadron colliders (see, e.g., [1,8–24]).

In the simplest models such as the sequential Standard Model (SSM) [8], new neutral Z'_{SSM} and charged W'_{SSM} bosons have couplings to fermions that are identical to those of the SM Z and W bosons but for which the trilinear couplings $Z'WW$ and $W'WZ$ are absent. The SSM has been used as a reference for experimental Z' and W' searches for decades, and the results can be reinterpreted in the context of other models; it is therefore useful for comparing the sensitivity of different experiments. Another class of models considered here are those inspired by grand unified theories, which are motivated by gauge unification or a restoration of the left-right symmetry violated by the weak interaction. Examples considered in this paper include the Z' bosons of the E_6-motivated [14] theories containing Z'_ψ, Z'_η, and Z'_χ and high-mass neutral bosons of the left-right (LR) symmetric extensions of the SM, based on the $SU(2)_L \otimes SU(2)_R \otimes U(1)_{B-L}$ gauge group, where $B - L$ refers to the difference between baryon and lepton numbers.

The data we consider were collected with the ATLAS and CMS detectors during the 2015–2018 running period of the LHC, referred to as run 2 and corresponding to a time-integrated luminosity of 139–140 fb^{-1}. The ATLAS experiment has presented the first search for dilepton resonances based on the full run 2 dataset [2,7] and set limits on the Z' and W' production cross sections times the branching fraction in the processes (1) and (2), $\sigma(pp \to Z'X) \times \mathrm{BR}(Z' \to \ell^+\ell^-)$ and $\sigma(pp \to W'X) \times \mathrm{BR}(W' \to \ell\nu)$, respectively, for $M_{Z'}$ and $M_{W'}$ in the 0.25–6 and 0.15–7 TeV ranges, correspondingly. Recently, similar searches have also been presented by the CMS Collaboration using 140 fb^{-1} of data recorded at $\sqrt{s} =$ 13 TeV [4]. The ATLAS and CMS Collaborations set a 95% confidence level (C.L.) lower limit on the Z' mass of ~4.6 to 5.2 TeV depending on the model [2,4] and 6.0 TeV for the W'_{SSM} [7].

Alternative Z' and W' search channels are the diboson reactions

$$pp \to Z'X \to WWX \tag{3}$$

and

$$pp \to W'X \to WZX. \tag{4}$$

The study of gauge boson pair production offers a powerful test of the spontaneously broken gauge symmetry of the SM and can be used as a probe for new phenomena beyond the SM. Specifically, in contrast to the DY processes (1) and (2), diboson reactions are not the primary discovery channels but can help to understand the origin of new gauge bosons.

As mentioned above, heavy resonances that can decay to gauge boson pairs are predicted in many scenarios of new physics, including extended gauge models (EGM) [8,25], models of warped extra dimensions [26,27], technicolor models [28,29] associated with technirho and other technimesons, composite Higgs models [30,31], and the heavy vector-triplet model [32], which generalizes a large number of models that predict spin-1 neutral (Z') and charged (W') resonances. In the SSM, the coupling constants of the $Z'(W')$ boson with SM fermions are the direct transcription of the corresponding SM couplings, while the $Z'(W')$ coupling to $WW(WZ)$ is strongly suppressed, $g_{Z'WW} = 0$ and $g_{W'WZ} = 0$. This suppression may arise naturally in an EGM: If the new gauge bosons and the SM ones belong to different gauge groups, a vertex such as $Z'WW$ ($W'WZ$) is forbidden. They can be induced only after symmetry breaking due to mixing of the gauge eigenstates. Searches for exotic heavy particles that decay into WW or WZ pairs are complementary to searches in the leptonic channels $\ell^+\ell^-$ and $\ell\nu$ of the processes (1) and (2). Moreover, there are models in which new gauge boson couplings to SM fermions are suppressed, giving rise to a fermiophobic Z' and W' with an enhanced coupling to electroweak gauge bosons [1,33]. It is therefore important to search for Z' and W' bosons also in the WW and WZ final states.

The properties of possible Z' and W' bosons are also constrained by measurements of electroweak (EW) processes at low energies, i.e., at energies much below their masses. Such bounds on the Z-Z' (W-W') mixing are mostly due to the constraints on deviation in Z (W) properties from the SM predictions. In particular, limits from direct hadron production with subsequent diboson decay at the Tevatron [34] and from virtual effects at the Large Electron-Positron Collider (LEP), through interference or mixing with the Z boson, imply that any new Z' boson is rather heavy and mixes very little with the Z boson. At LEP and the Stanford Linear Collider, the mixing angle is strongly constrained by very high-precision Z pole experiments [35]. These include measurements of the Z line shape and the leptonic branching ratios as well as leptonic forward-backward asymmetries. The measurements show that the mixing angles, referred to as $\xi_{Z\text{-}Z'}$

and $\xi_{W\text{-}W'}$, between the gauge eigenstates must be smaller than about 10^{-3} and 10^{-2}, respectively [1,15].

Previous analyses of the Z-Z' and W-W' mixing [36–38] were carried out using the diboson and dilepton production datasets corresponding to the time-integrated luminosity of ~36 fb^{-1} collected in 2015 and 2016 with the ATLAS and CMS Collaborations at $\sqrt{s} = 13$ TeV where, in the former case, electroweak Z and W gauge bosons decay into the semileptonic channel [39] or into the dijet final state [40]. The results of the present analysis benefit from the increased size of the data sample, now amounting to an integrated luminosity of 139 fb^{-1} recorded by the ATLAS detector in run 2 [41–44], almost 4 times larger than what was available for the previous study.[1] In addition, further improvement in placing limits on the Z' and W' mass and Z-Z' and W-W' mixing parameters can be achieved in semileptonic WW/WZ final states in which one vector boson decays leptonically ($Z \to \ell\ell, \nu\nu, W \to \ell\nu$) while the other decays hadronically ($Z/W \to qq$).[2] Also, here we extend our analysis presented in Ref. [45], where we utilized the full run 2 ATLAS dataset for EGM (SSM) to various Z' models, including E_6-based Z_χ, Z_ψ, Z_η, and also Z_{LR} boson appearing in models with left-right symmetry. Thus, our present analysis is complementary to the previous studies [45].

We present results as constraints on the relevant Z-Z' (W-W') mixing angle, $\xi_{Z\text{-}Z'}$ ($\xi_{W\text{-}W'}$), and on the mass $M_{Z'}$ ($M_{W'}$) and display the combined allowed parameter space for the benchmark Z' (W') models, showing also indirect constraints from electroweak precision data. Previous direct search constraints from the Tevatron and from the LHC with 7 and 8 TeV in run 1 (where available) are compared to those obtained from the LHC at 13 TeV with the full ATLAS run 2 dataset of a time-integrated luminosity of 139 fb^{-1} in the semileptonic [43,44] and fully hadronic ($qqqq$) [41] final states.

The paper is structured as follows. In Sec. II, we present the theoretical framework; then, in Sec. III, we summarize the relevant cross sections for the diboson and dilepton production processes (3) and (1) in the narrow-width approximation (NWA). Next, we discuss the relevant Z' widths and branching ratios within the considered benchmark models. Furthermore, we present an analysis of bounds on Z-Z' mixing from constraints on diboson and dilepton production in the context of the benchmark models with an extended gauge sector, employing the most recent searches recorded by the ATLAS (139 fb^{-1}) detector in the semileptonic [43,44] and fully hadronic (referred to as $qqqq$) [41,42] final states at the LHC. Then, we show the resulting constraints on the $M_{Z'} - \xi_{Z\text{-}Z'}$ parameter space obtained from these processes. Furthermore, we collect and compare the indirect constraints obtained from electroweak precision data, direct search constraints derived from the LHC in run 1 and early run 2 data. In Sec. IV, we present the corresponding analysis of bounds on W-W' mixing, performed in a similar fashion as for the Z', from constraints on diboson and dilepton production processes (4) and (2) in the context of the EGM. Section V presents some concluding remarks.

[1]In the current analysis, we utilize the full run 2 ATLAS dataset on diboson resonance production [41,43,44], rather than that of CMS, as the latter one is unavailable so far.

[2]To simplify notation, antiparticles are denoted by the same symbol as the corresponding particles.

II. MIXING AND PARAMETERS

We consider Z-Z' mixing within the framework of models with an extended gauge sector such as the E_6 models, the LR model, and the EGM (see, e.g., [8,14–17]). The mass eigenstates Z and Z' are admixtures of the weak eigenstates Z^0 of $SU(2) \times U(1)$ and $Z^{0\prime}$ of the extra $U(1)'$, respectively:

$$Z = Z^0 \cos\phi + Z^{0\prime} \sin\phi, \tag{5a}$$

$$Z' = -Z^0 \sin\phi + Z^{0\prime} \cos\phi. \tag{5b}$$

For each type of Z' boson, defined by its gauge couplings, there are three classes of models, which differ in the assumptions concerning the quantum numbers of the Higgs fields which generate the Z-boson mass matrix [14,15]. In each case, there is a relation between the Z^0-$Z^{0\prime}$ mixing angle ϕ and the masses M_Z and $M_{Z'}$ [14]:

$$\tan^2\phi = \frac{M_{Z^0}^2 - M_Z^2}{M_{Z'}^2 - M_{Z^0}^2} \simeq \frac{2M_{Z^0}\Delta M}{M_{Z'}^2}, \tag{6}$$

where the downward shift $\Delta M = M_{Z^0} - M_Z > 0$ and M_{Z^0} is the mass of the Z boson in the absence of mixing, i.e., for $\phi = 0$, given by

$$M_{Z^0} = \frac{M_W}{\sqrt{\rho_0}\cos\theta_W}. \tag{7}$$

The mixing angle ϕ will play an important role in our analysis. Such mixing effects reflect the underlying gauge symmetry and/or the Higgs sector of the model, as the ρ_0 parameter depends on the ratios of Higgs vacuum expectation values and on the total and third components of weak isospin of the Higgs fields. We set $\rho_0 = 1$ here; this corresponds to a Higgs sector with only $SU(2)$ doublets and singlets [14]. Once we assume the mass M_Z to be determined experimentally, the mixing depends on two free parameters, which we identify as ϕ and $M_{Z'}$, a parametrization that we will adopt throughout the paper.

This Z^0-$Z^{0\prime}$ mixing induces a change in the couplings of the two bosons to fermions. From Eq. (5), one obtains the

vector and axial-vector couplings of the Z and Z' bosons to fermions:

$$v_f = v_f^0 \cos\phi + v_f^{0\prime} \sin\phi, \qquad a_f = a_f^0 \cos\phi + a_f^{0\prime} \sin\phi, \tag{8a}$$

$$v_f' = v_f^{0\prime} \cos\phi - v_f^0 \sin\phi, \qquad a_f' = a_f^{0\prime} \cos\phi - a_f^0 \sin\phi, \tag{8b}$$

with unprimed and primed couplings referring to Z^0 and $Z^{0\prime}$, respectively, and found, e.g., in Ref. [17].

An important property of the models under consideration is that the gauge eigenstate $Z^{0\prime}$ does not couple to the W^+W^- pair, since it is neutral under $SU(2)$. Therefore, the W-pair production is sensitive to a Z' only in the case of a nonzero Z^0-$Z^{0\prime}$ mixing. From Eq. (5), one obtains

$$g_{WWZ} = \cos\phi g_{WWZ^0}, \tag{9a}$$

$$g_{WWZ'} = -\sin\phi g_{WWZ^0}, \tag{9b}$$

where $g_{WWZ^0} = e\cot\theta_W$. Also, $g_{WW\gamma} = e$.

In many extended models, while the couplings to fermions do not differ much from those of the SM, the $Z'WW$ coupling is substantially suppressed with respect to that of the SM. In fact, in the extended gauge models, the SM trilinear gauge boson coupling strength g_{WWZ^0} is replaced by $g_{WWZ^0} \to \xi_{Z\text{-}Z'} \cdot g_{WWZ^0}$, where $\xi_{Z\text{-}Z'} \equiv |\sin\phi|$ [see Eq. (9b)] is the mixing factor.[3] We will set cross section limits on such Z' as functions of the mass $M_{Z'}$ and ξ.

In addition, we study W-W' mixing in the process (4) within the framework of the EGM model [8,25]. At the tree level, mass mixing may be induced between the electrically charged gauge bosons. The physical (mass) eigenstates of W and W' are admixtures of the weak eigenstates denoted as $\hat{W}$ and $\hat{W}'$, respectively, and obtained by a rotation of those fields [1,13]:

$$W^\pm = \hat{W}^\pm \cos\theta + \hat{W}'^\pm \sin\theta, \tag{10a}$$

$$W'^\pm = -\hat{W}^\pm \sin\theta + \hat{W}'^\pm \cos\theta, \tag{10b}$$

in analogy with Eq. (5). Upon diagonalization of their mass matrix, the couplings of the observed W boson are shifted from the SM values.

The properties of possible Z' and W' bosons, apart from collider experiments, are also constrained by measurements of EW processes at low energies, i.e., at energies much below their masses. Such bounds on the Z-Z' (W-W') mixing are mostly due to the constraints on the deviation in Z (W) properties compared to the SM predictions. These measurements show that the mixing angles $\xi_{Z\text{-}Z'}$ and $\xi_{W\text{-}W'}(\equiv|\sin\theta|)$ between the gauge eigenstates must be smaller than $\sim 10^{-3}$ and 10^{-2} [1], respectively.

[3]For weak mixing, $\xi_{Z\text{-}Z'} \simeq |\phi|$ and is, therefore, often referred to as a mixing "angle."

III. Z' PRODUCTION AND DECAY IN pp COLLISION

We shall first consider Z' production in some detail and subsequently turn to the W' case. In some sense, the Z' sector is richer than the W' sector; different models predict different ratios of the vector and axial-vector couplings. The W' models, on the other hand, will all be restricted in the choice of pure left-handed couplings to fermions. Among the Z' models, we start out with a detailed discussion of the ψ model.

A. Z' resonant production cross section

The Z' production and subsequent decay into WW in proton-proton collisions occurs via quark-antiquark annihilation in the s channel. The cross section of the process (3) can at the LHC be observed through resonant pair production of gauge bosons WW. Using the NWA, one can factorize the process (3) into the Z' production and its subsequent decay:

$$\sigma(pp \to Z'X \to WWX) = \sigma(pp \to Z'X) \times \mathrm{BR}(Z' \to WW). \tag{11}$$

Here, $\sigma(pp \to Z'X)$ is the total (theoretical) Z' production cross section and $\mathrm{BR}(Z' \to WW) = \Gamma_{Z'}^{WW}/\Gamma_{Z'}$ with $\Gamma_{Z'}$ the total width of the Z'. "Narrow" refers to the assumption that the natural width of the resonance is smaller than the typical experimental resolution of 5% of its mass [46,47]. This is valid for a large fraction of the parameter space of the considered models.

B. The Z' width

In the calculation of the total width $\Gamma_{Z'}$, we consider the following channels: $Z' \to f\bar{f}$, W^+W^-, and ZH [36,37,45,48], where H is the SM Higgs boson and f refers to the SM fermions ($f = l, \nu, q$). Throughout the paper, we shall ignore the couplings of the Z' to any beyond-SM particles such as right-handed neutrinos, which we take to be heavier than $M_Z'/2$, as well as to supersymmetry (SUSY) partners and any other exotic fermions. Such additional states may all together increase the width of the Z' by up to about a factor of 5 [49] and, hence, lower the branching ratio into a W^+W^- pair by the same factor.

The total width $\Gamma_{Z'}$ of the Z' boson can then be written as follows:

$$\Gamma_{Z'} = \sum_f \Gamma_{Z'}^{ff} + \Gamma_{Z'}^{WW} + \Gamma_{Z'}^{ZH}. \tag{12}$$

TABLE I. Ratio $\Gamma^{ff}_{Z'}/M_{Z'}$ for the χ, ψ, η, LR, and EGM models.

Z'	$\Gamma^{ff}_{Z'}/M_{Z'}$ [%]
χ	1.2
ψ	0.5
η	0.6
LR	2.0
EGM	3.0

The two last terms, which are often neglected in studies at low and moderate values of $M_{Z'}$, are due to Z-Z' mixing. For the range of $M_{Z'}$ values below ~3 to 4 TeV, the dependence of $\Gamma_{Z'}$ on the values of $\xi_{Z\text{-}Z'}$ (within its allowed range) is unimportant. Therefore, in this mass range, one can approximate the total width as $\Gamma_{Z'} \approx \sum_f \Gamma^{ff}_{Z'}$, where the sum runs over SM fermions only. The ratios of $\Gamma^{ff}_{Z'}/M_{Z'}$ for the benchmark models are summarized in Table I. One can appreciate the narrowness of the $Z_{Z'}$ pole from Table I.

However, for larger Z' masses, $M_{Z'} > 4$ TeV, there is an enhancement in the coupling that cancels the suppression due to the tiny Z-Z' mixing parameter $\xi_{Z\text{-}Z'}$ [48]. We note that the "equivalence theorem" [50] suggests a value for $\mathrm{BR}(Z' \to ZH)$ comparable to $\mathrm{BR}(Z' \to W^+W^-)$, up to electroweak symmetry-breaking effects and phase-space factors. Throughout this paper, for definiteness, we adopt a scenario where both partial widths are comparable, $\Gamma^{ZH}_{Z'} \simeq \Gamma^{WW}_{Z'}$ for heavy $M_{Z'}$ [51–53].

For all $M_{Z'}$ values of interest for the LHC, the width of the Z' boson is considerably smaller than the experimental mass resolution ΔM for which we adopt the parametrization in reconstructing the diboson invariant mass of the W^+W^- system, $\Delta M/M \approx 5\%$, as proposed, e.g., in Refs. [46,47].[4]

The partial width of the $Z' \to W^+W^-$ decay channel can be written as [8]

$$\Gamma^{WW}_{Z'} = \frac{\alpha_{\mathrm{em}}}{48}\cot^2\theta_W M_{Z'}\left(\frac{M_{Z'}}{M_W}\right)^4\left(1-4\frac{M_W^2}{M_{Z'}^2}\right)^{3/2} \times\left[1+20\left(\frac{M_W}{M_{Z'}}\right)^2+12\left(\frac{M_W}{M_{Z'}}\right)^4\right]\cdot\xi^2_{Z\text{-}Z'}. \quad (13)$$

For a fixed mixing factor $\xi_{Z\text{-}Z'}$ and at large $M_{Z'}$, where $\Gamma^{WW}_{Z'}$ dominates over $\sum_f \Gamma^{ff}_{Z'}$, the total width increases rapidly with the mass $M_{Z'}$ because of the quintic dependence of the W^+W^- mode on the Z' mass as shown in Eq. (13). In this case, the W^+W^- mode (together with $Z' \to ZH$) becomes dominant and $\mathrm{BR}(Z' \to W^+W^-) \to 0.5$ (this value arises from the assumption $\Gamma^{ZH}_{Z'} = \Gamma^{WW}_{Z'}$), while the fermionic decay channels ($\Gamma^{ff}_{Z'} \propto M_{Z'}$) are increasingly suppressed. These features are illustrated in Fig. 2, where we plot

[4]This ΔM should not be confused with that of Eq. (6).

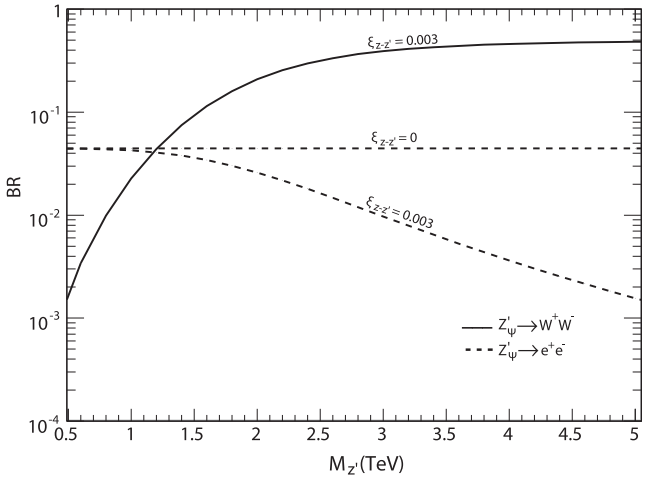

FIG. 2. Branching ratio $\mathrm{BR}(Z' \to W^+W^-)$ (solid line) and $\mathrm{BR}(Z' \to e^+e^-)$ (dashed line) vs $M_{Z'}$ in the Z'_ψ model for Z-Z' mixing factor $\xi_{Z\text{-}Z'} = 0$ and $\xi_{Z\text{-}Z'} = 3 \times 10^{-3}$. It is assumed that $\Gamma^{ZH}_{Z'} = \Gamma^{WW}_{Z'}$.

$\mathrm{BR}(Z' \to W^+W^-)$ and $\mathrm{BR}(Z' \to e^+e^-)$ vs $M_{Z'}$ for the Z'_ψ model.

C. Hadron production and diboson decay of Z'

In Fig. 3, we consider the full ATLAS run 2 dataset of a time-integrated luminosity of 139 fb^{-1} and show the observed 95% C.L. upper limits on the production cross section times the branching fraction, $\sigma_{95\%} \times \mathrm{BR}(Z' \to W^+W^-)$, as a function of the Z' mass, obtained from the semileptonic [43,44] and fully hadronic ($qqqq$) [41,42] final states. This allows for a comparison of the sensitivities of the data to mixing parameters and new gauge boson mass. This comparison demonstrates the dominating sensitivity to Z' of the semileptonic channel with respect to the fully hadronic one, over almost the whole Z' mass range.

Then, for Z'_ψ we compute the LHC production cross section multiplied by the branching ratio into two W bosons, $\sigma(pp \to Z'_\psi X) \times \mathrm{BR}(Z'_\psi \to W^+W^-)$, as a function of the two parameters ($M_{Z'}$, $\xi_{Z\text{-}Z'}$), and compare it with the limits established by the ATLAS experiment, $\sigma_{95\%} \times \mathrm{BR}(Z' \to W^+W^-)$. The SM backgrounds have been carefully evaluated by the experimental collaborations and accounted for in $\sigma_{95\%} \times \mathrm{BR}(Z' \to W^+W^-)$. Therefore, in our analysis, we simulate only the Z'_ψ signal.

In Fig. 3, the theoretical production cross section $\sigma(pp \to Z'_\psi) \times \mathrm{BR}(Z'_\psi \to W^+W^-)$ for the Z'_ψ boson is calculated from a dedicated modification of PYTHIA8.2 [54]. As mentioned above, higher-order QCD corrections to the signal were estimated using a K factor, for which we adopt a mass-independent value of 1.9 [55–57]. These theoretical curves for the cross sections, in descending order, correspond to values of the Z-Z' mixing factor $\xi_{Z\text{-}Z'}$ ranging from 3×10^{-3} down to 3×10^{-4}. The intersection points of the measured upper limits on the production cross

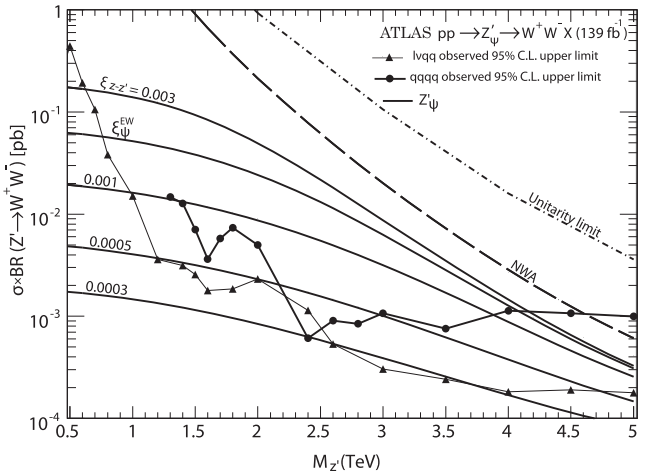

FIG. 3. Observed 95% C.L. upper limits on the production cross section times the branching fraction $\sigma_{95\%} \times \mathrm{BR}(Z' \to W^+W^-)$ as a function of the Z' mass $M_{Z'}$, showing ATLAS data for the semileptonic (thin solid line) [43,44] and fully hadronic (thick solid line) [41] final states for 139 fb^{-1}. Theoretical production cross sections $\sigma(pp \to Z'_\psi + X) \times \mathrm{BR}(Z'_\psi \to W^+W^-)$ are shown for mixing factors $\xi_{Z\text{-}Z'}$ ranging from 3×10^{-3} down to 3×10^{-4}. Also, the cross section solid line labeled ξ_ψ^{EW} corresponds to the mixing parameter $\xi_{Z'}^{\mathrm{EW}}$ indicated in Table II for the Z'_ψ model. The area lying below the long-dashed curve labeled NWA corresponds to the region where the Z' resonance width is predicted to be less than 5% of the resonance mass, in which the narrow-width assumption is satisfied. The lower boundary of the region excluded by the unitarity constraints is also indicated.

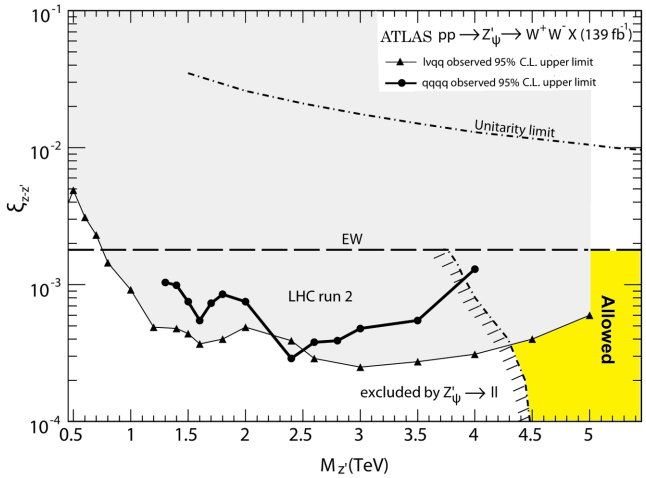

FIG. 4. The Z'_ψ model: 95% C.L. exclusion regions in the two-dimensional ($M_{Z'}$, $\xi_{Z\text{-}Z'}$) plane obtained after incorporating indirect constraints from electroweak precision data (horizontal dashed straight line labeled "EW") and direct search constraints from the LHC search for $pp \to Z' \to WW$ in semileptonic final states using the full run 2 ATLAS dataset. Limits obtained from the hadronic channel $qqqq$ are overlaid for comparison. The region above each curve for the WW channel is excluded. The steep curve labeled "excluded by $Z'_\psi \to \ell\ell$" shows the exclusion based on the dilepton channel $pp \to Z'_\psi \to \ell\ell + X$. The unitarity limit is shown as the dot-dashed curve. The overall allowed region is shown as a yellow area.

section with this theoretical cross section for various values of $\xi_{Z\text{-}Z'}$ give the corresponding lower bounds on ($M_{Z'}$, $\xi_{Z\text{-}Z'}$), presented in Fig. 4.

Different bounds on the Z' parameter space are collected in Fig. 4 for the Z'_ψ model, showing that, at high masses, the limits on $\xi_{Z\text{-}Z'}$ obtained from the full run 2 dataset collected at $\sqrt{s} = 13$ TeV and recorded by the ATLAS detector are substantially stronger than that derived from the global analysis of the precision electroweak data [15], which is also displayed. Limits obtained separately from the individual semileptonic channel $\ell\nu qq$ and the fully hadronic cannel $qqqq$ are shown for comparison. It turns out that the semileptonic channel dominates the sensitivity over almost the whole resonance mass range 0.5 TeV $\leq M_{Z'} \leq$ 5 TeV, while in the rather narrow mass range 2.2 TeV $\leq M_{Z'} \leq$ 2.5 TeV the all-hadronic channel is most sensitive.

D. Z-Z' mixing effects in dilepton decay of $Z' \to \ell\ell$

The above analysis was for the diboson process (3), employing one of the most recent ATLAS searches for semileptonic [43,44] and fully hadronic [41] final states. Next, we turn to the dilepton production process (1); this process gives valuable complementary information.

We compute the Z' theoretical production cross section at the LHC, $\sigma(pp \to Z'X)$, multiplied by the branching ratio into two leptons, $\ell\ell$ ($\ell = e$, μ), i.e., $\sigma(pp \to Z'X) \times \mathrm{BR}(Z' \to \ell\ell)$, as a function of $M_{Z'}$, and compare it with the upper limits established by the experiment [2] for 139 fb^{-1}. We make use of the relevant set of tables and figures (including additional results for dielectron and dimuon channels) available at the Durham HepData repository [3].

Results for $\sigma_{95\%} \times \mathrm{BR}(Z' \to \ell\ell)$ are shown in Fig. 5. To account for next-to-next-to-leading order (NNLO) effects in the QCD strong coupling constant, the leading order (LO) cross sections calculated with PYTHIA8.2 [54] are multiplied by a mass-independent K factor. The value of the K factor is estimated at a dilepton invariant mass of ~3.0 to 4.5 TeV and found to be consistent with unity [58,59].

For illustrative purposes, we show theoretical production cross sections $\sigma(pp \to Z'X) \times \mathrm{BR}(Z' \to \ell\ell)$ for the ψ model Z', given by the dashed curves in Fig. 5. These curves, in descending order, correspond to values of the mixing factor $\xi_{Z\text{-}Z'}$ from 0 to 5×10^{-3}. Qualitatively, the decrease of the theoretical cross section with increasing values of $\xi_{Z\text{-}Z'}$ can be understood as follows: For increasing $\xi_{Z\text{-}Z'}$, the $Z' \to W^+W^-$ mode will at high mass $M_{Z'}$ become more dominant (as illustrated in Fig. 2), and $\mathrm{BR}(Z' \to \ell\ell)$ will decrease correspondingly. Notice also that, applying a mass-dependent K factor (which for this process is less than

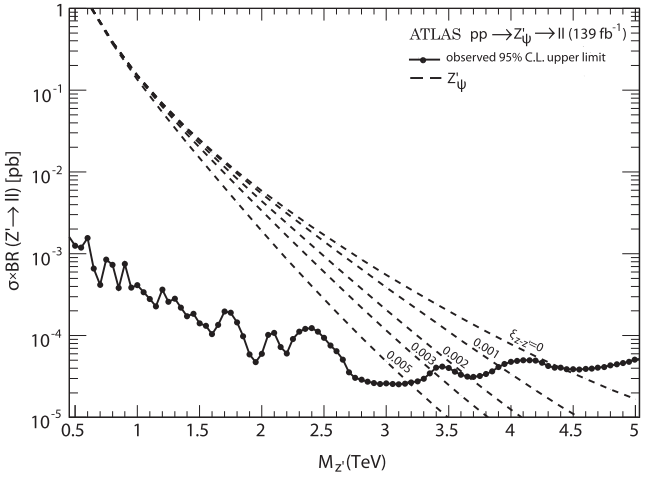

FIG. 5. Solid line: observed 95% C.L. upper bound on the Z' production cross section times the branching ratio to two leptons, $\sigma_{95\%} \times \mathrm{BR}(Z' \to \ell\ell)$, where $\ell = e, \mu$, obtained at the LHC with integrated luminosity $\mathcal{L}_{\mathrm{int}} = 139$ fb^{-1} by the ATLAS Collaboration [2,3]. Results are shown for the combined dilepton channel. Dashed lines: theoretical production cross section $\sigma(pp \to Z') \times \mathrm{BR}(Z' \to \ell\ell)$ for the Z' boson in the ψ model, calculated from PYTHIA8.2 with an NNLO K factor. These curves in descending order correspond to values of the Z-Z' mixing factor $\xi_{Z\text{-}Z'}$ from 0 to 0.005.

1.04), the ψ model mass limit of the Z' changes by only $\sim\mathcal{O}(50\ \mathrm{GeV})$, justifying the use of the simpler mass-independent K factor [58,59].

Comparison of $\sigma(pp \to Z'X) \times \mathrm{BR}(Z' \to \ell\ell)$ vs $\sigma_{95\%} \times \mathrm{BR}(Z' \to \ell\ell)$ displayed in Fig. 5 permits us to read off an allowed mixing for a given mass value; higher masses are allowed for smaller mixing, for the reason stated above. This analysis of Z-Z' mixing, illustrated here for the ψ model, can also be performed for the other benchmark models. The results of the numerical analysis for these tested models are presented in Figs. 6–9. Mass limits are calculated as the intersection between the observed limits with the model prediction. Table II lists the mass limits for two representative cases, namely, for vanishing mixing ($\xi_{Z\text{-}Z'} = 0$) and for the mixing $\xi^{\mathrm{EW}}_{Z\text{-}Z'}$ derived from the electroweak precision data [15]. The former are consistent with those derived in Refs. [2,4], whereas the mass limits at $\xi^{\mathrm{EW}}_{Z\text{-}Z'}$ are weaker by ∼10%–30%.

As described above, both the diboson mode and the dilepton process yield limits on the $(M_{Z'}, \xi_{Z\text{-}Z'})$ parameter space. These are rather complementary, as shown in Fig. 4, where we collect these limits for the ψ model. The limits arising from the diboson channel are basically excluding large values of $\xi_{Z\text{-}Z'}$, strongest at intermediate masses $M_{Z'} \sim 2$–4 TeV. The limits arising from the dilepton channel, on the other hand, basically exclude masses $M_{Z'} \lesssim 4.5$ TeV, with only a weak dependence on $\xi_{Z\text{-}Z'}$. For reference, we plot also a curve labeled "unitarity limit" that corresponds to the unitarity bound [37,60]. In Ref. [60], it was shown that the saturation of unitarity in the elastic scattering $W^+W^- \to W^+W^-$ leads to the constraint $(g_{Z'WW})_{\max} = g_{ZWW} \cdot (M_Z/\sqrt{3}M_{Z'})$ that was adopted here.

For comparison, we show in Fig. 9 (for the EGM model) also the exclusion reach expected at the end of run 3 (300 fb^{-1}) at the LHC, as well as at the HL-LHC (3000 fb^{-1}) [61], which illustrates the corresponding extension of the excluded limits on $\xi_{Z\text{-}Z'}$ down to 2.0×10^{-4} and 1.1×10^{-4}, respectively, within the Z' mass range under study. Furthermore, the expected lower limit on the Z' mass can be set from the dilepton production at higher luminosity. The current Z'_{EGM} mass limit of 5.1 TeV at $\xi_{Z\text{-}Z'} = 0$ obtained using 139 fb^{-1} of data will extend to 6.7 TeV [62].

In Table III, we collect our limits on the Z' parameters for the benchmark models. Also shown in Table III are the limits on the Z-Z' (W-W') mixing parameter $\xi_{Z\text{-}Z'}$ ($\xi_{W\text{-}W'}$) from studies of diboson WW (WZ) pair production at the Tevatron. Table III shows that the limits on $\xi_{Z\text{-}Z'}$ from the EW precision data are generally competitive with the future collider, ILC@0.5 TeV, but in many cases, they are stronger than those from the Tevatron.

The diboson production at the LHC@13 TeV allows us to place stringent constraints on the Z-Z' mixing angle and Z' mass $M_{Z'}$. We imposed limits on the mass and the Z-Z' mixing angle of the Z' bosons by using data comprised of pp collisions at $\sqrt{s} = 13$ TeV and recorded by the ATLAS detectors at the CERN LHC, with integrated luminosities of ∼139 fb^{-1} from run 2 data taking.

Also, we show that the derived constraints on the Z-Z' mixing angle for the benchmark models are of the order of a few $\times 10^{-4}$ and they are greatly improved with respect to those derived from the global analysis of electroweak data. In addition, we demonstrated in Fig. 9 that further improvement on the constraining of this mixing can be achieved from the analysis of data to be collected at higher luminosity expected in the run 3 and HL-LHC options. We also show that only the future e^+e^- linear collider ILC with polarized beams and with very high energy and luminosity, $\sqrt{s} = 1$ TeV and $\mathcal{L}_{\mathrm{int}} = 1$ ab^{-1}, may have a chance to compete with the current LHC sensitivity to the mixing angle in run 2 but will not reach the levels of the run 3 and HL-LHC options.

IV. W' PRODUCTION AND DECAY IN pp COLLISION

In contrast to the rich spectrum of Z' models considered above, with different vector and axial-vector couplings, for W' we consider only $V - A$ couplings to fermions.

A. W' resonant production cross section

We consider the simplest EGM model which predicts charged heavy gauge bosons. The analysis of W-W' mixing

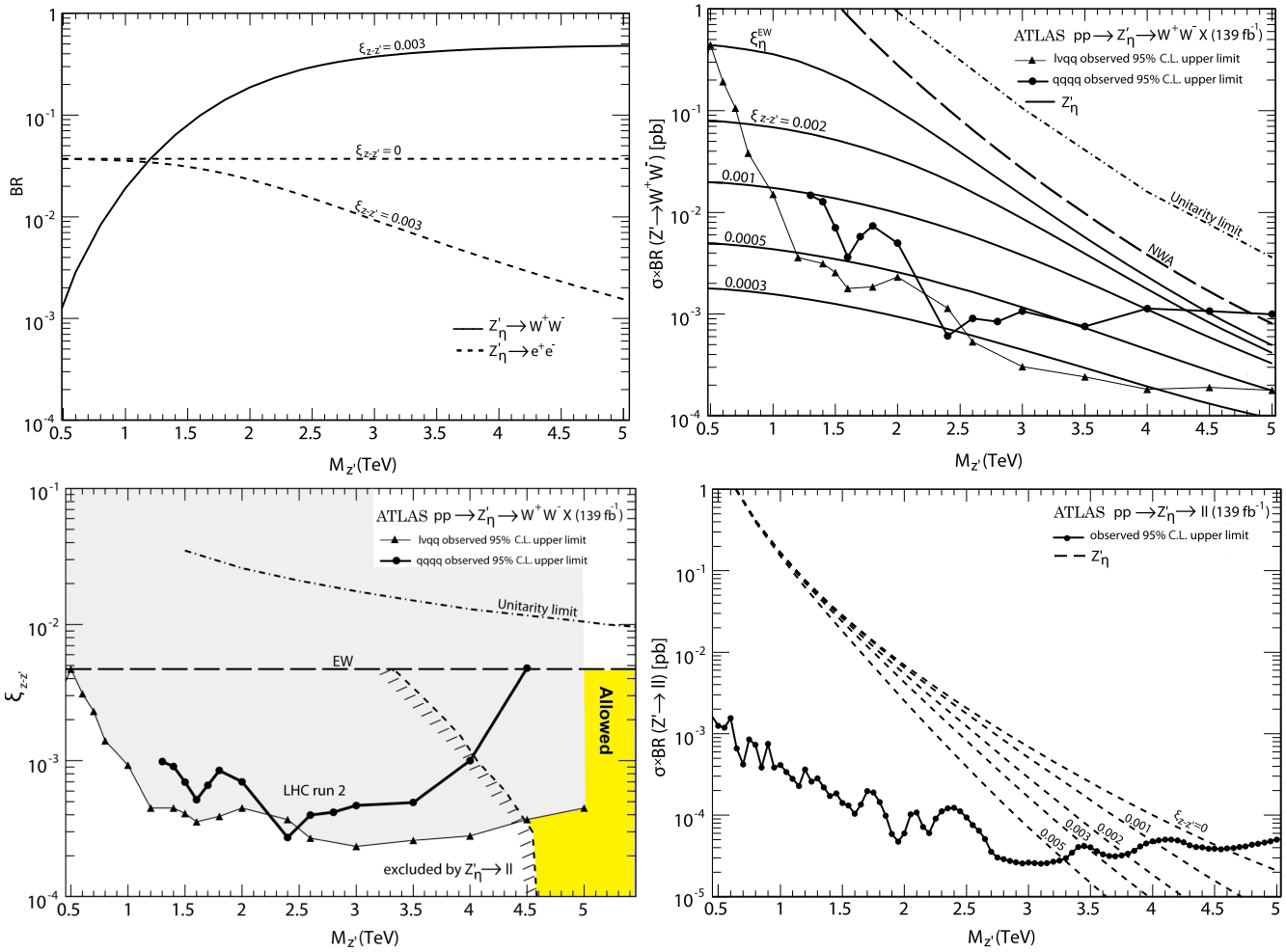

FIG. 6. The Z'_η model. Top-left, top-right, bottom-left, and bottom-right panels: analogous to Figs. 2, 3, 4, and 5, respectively.

in diboson and dilepton pair production which will be performed below is quite analogous to that carried out in previous sections for Z-Z' mixing. At lowest order in the EGM, W' production and decay into WZ in proton-proton collisions occurs through quark-antiquark annihilation in the s channel. Using the NWA, one can factorize the process (4) into the W' production and the W' decay:

$$\sigma(pp \to W'X \to WZX) = \sigma(pp \to W'X) \times \mathrm{BR}(W' \to WZ). \quad (14)$$

Here, $\sigma(pp \to W'X)$ is the total (theoretical) W' production cross section and $\mathrm{BR}(W' \to WZ) = \Gamma^{WZ}_{W'}/\Gamma_{W'}$ with $\Gamma_{W'}$ the total width of the W'.

B. The W' width

In the EGM, the W' bosons can decay into SM fermions, gauge bosons (WZ), or WH. In the calculation of the total width $\Gamma_{W'}$, we consider the following channels: $W' \to f\bar{f}'$, WZ, and WH, where f is a SM fermion ($f = \ell, \nu, q$).[5] Only left-handed neutrinos are considered; possible right-handed neutrinos are assumed to be kinematically unavailable as final states. Also, like for the Z' case, we shall ignore the couplings to other beyond-SM particles such as SUSY partners and exotic fermions. As a result, the total decay width of the W' boson is taken to be

$$\Gamma_{W'} = \sum_f \Gamma^{f\bar{f}'}_{W'} + \Gamma^{WZ}_{W'} + \Gamma^{WH}_{W'}. \quad (15)$$

Like for the Z' case, the presence of the last two decay channels, which are often neglected at low and moderate values of $M_{W'}$, is due to W-W' mixing which is constrained to be tiny. In particular, for the range of $M_{W'}$ values below ~1.0 to 1.5 TeV, the dependence of $\Gamma_{W'}$ on the values of $\xi_{W\text{-}W'}$ (within its allowed range) induced by $\Gamma^{WZ}_{W'}$ and $\Gamma^{WH}_{W'}$ is unimportant, because $\sum_f \Gamma^{f\bar{f}'}_{W'}$ dominates over the diboson

[5]Here, in contrast to the Z' case, the ℓ includes τ leptons.

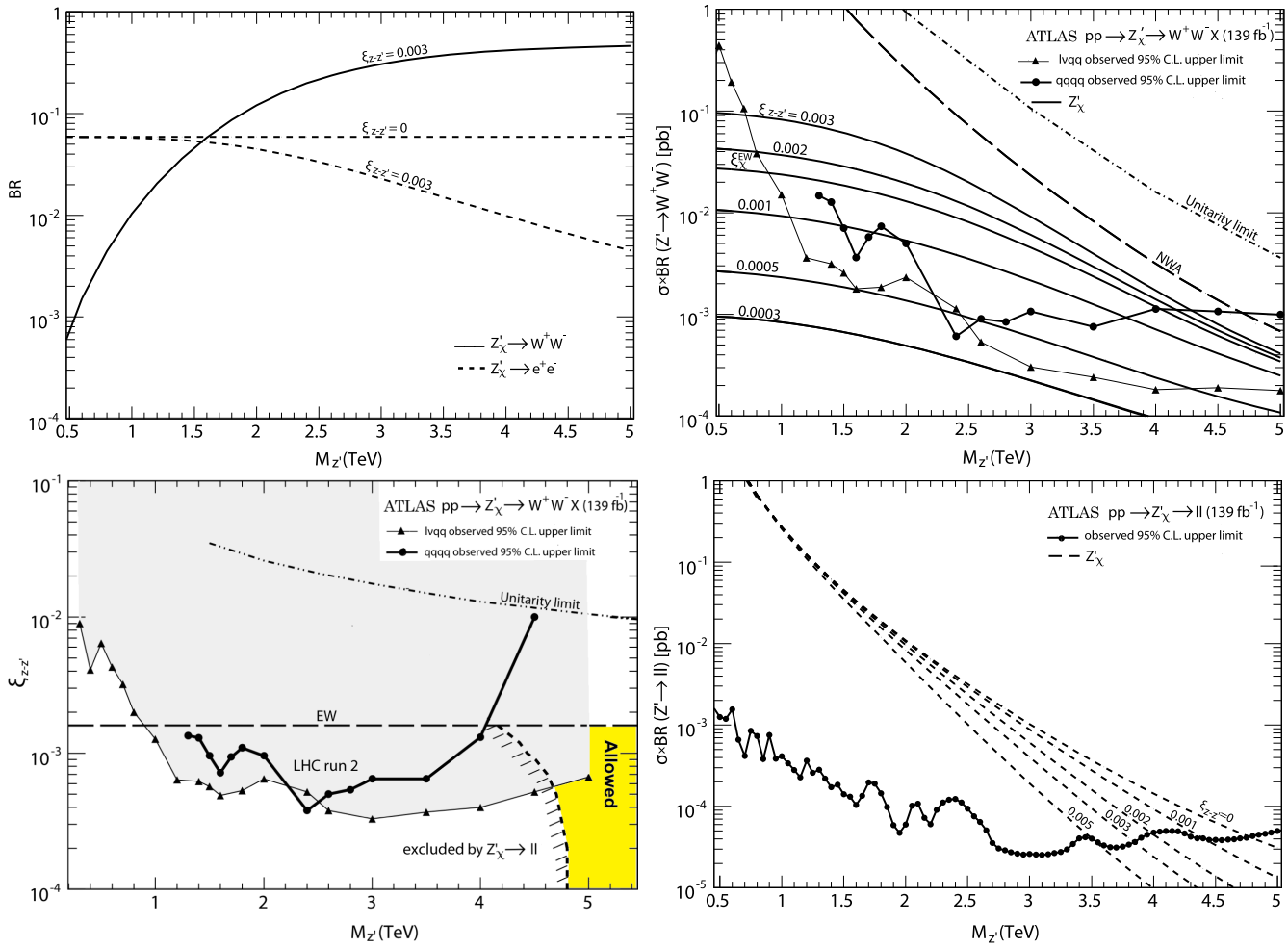

FIG. 7. The Z'_χ model. Top-left, top-right, bottom-left, and bottom-right panels: analogous to Figs. 2, 3, 4, and 5, respectively.

partial widths. Therefore, in this mass range, one can approximate the total width as $\Gamma_{W'} \approx \sum_f \Gamma^{f\bar{f}'}_{W'} = 3.5\% \times M_{W'}$ [38], where the sum runs over SM fermions only.

For heavier W' bosons, the diboson decay channels WZ and WH start to play an important role, and we are no longer able to ignore them [38,45]. To be specific, in analogy with the Z' case, we assume that both partial widths are comparable, $\Gamma^{WH}_{W'} \simeq \Gamma^{WZ}_{W'}$ for heavy $M_{W'}$, as required by the equivalence theorem [50].

The expression for the partial width of the $W' \to WZ$ decay channel in the EGM can be written as [8,38]

$$\Gamma^{WZ}_{W'} = \frac{\alpha_{\rm em}}{48}\cot^2\theta_W M_{W'} \frac{M^4_{W'}}{M^2_W M^2_Z}\left[\left(1-\frac{M^2_Z - M^2_W}{M^2_{W'}}\right)^2 - 4\frac{M^2_W}{M^2_{W'}}\right]^{3/2}\left[1+10\left(\frac{M^2_W+M^2_Z}{M^2_{W'}}\right)+\frac{M^4_W+M^4_Z+10M^2_W M^2_Z}{M^4_{W'}}\right]\cdot \xi^2_{W\text{-}W'}. \tag{16}$$

For a fixed mixing factor $\xi_{W\text{-}W'}$ and at large $M_{W'}$, the total width increases rapidly with the W' mass because of the quintic dependence of the WZ mode on the W' mass $\Gamma^{WZ}_{W'} \propto M_{W'}[M^4_{W'}/(M^2_W M^2_Z)]$, corresponding to the production of longitudinally polarized W and Z in the channel $W' \to W_L Z_L$ [8,38]. In this case, the WZ mode (as well as WH) becomes dominant and $\mathrm{BR}(W' \to WZ) \to 0.5$, while the fermionic decay channels $\sum_f \Gamma^{f\bar{f}'}_{W'} \propto M_{W'}$ are increasingly suppressed, as illustrated in Fig. 10 (left panel).

C. Hadron production and diboson decay of W'

Our analysis employs the recent searches for diboson processes in semileptonic final states provided by ATLAS

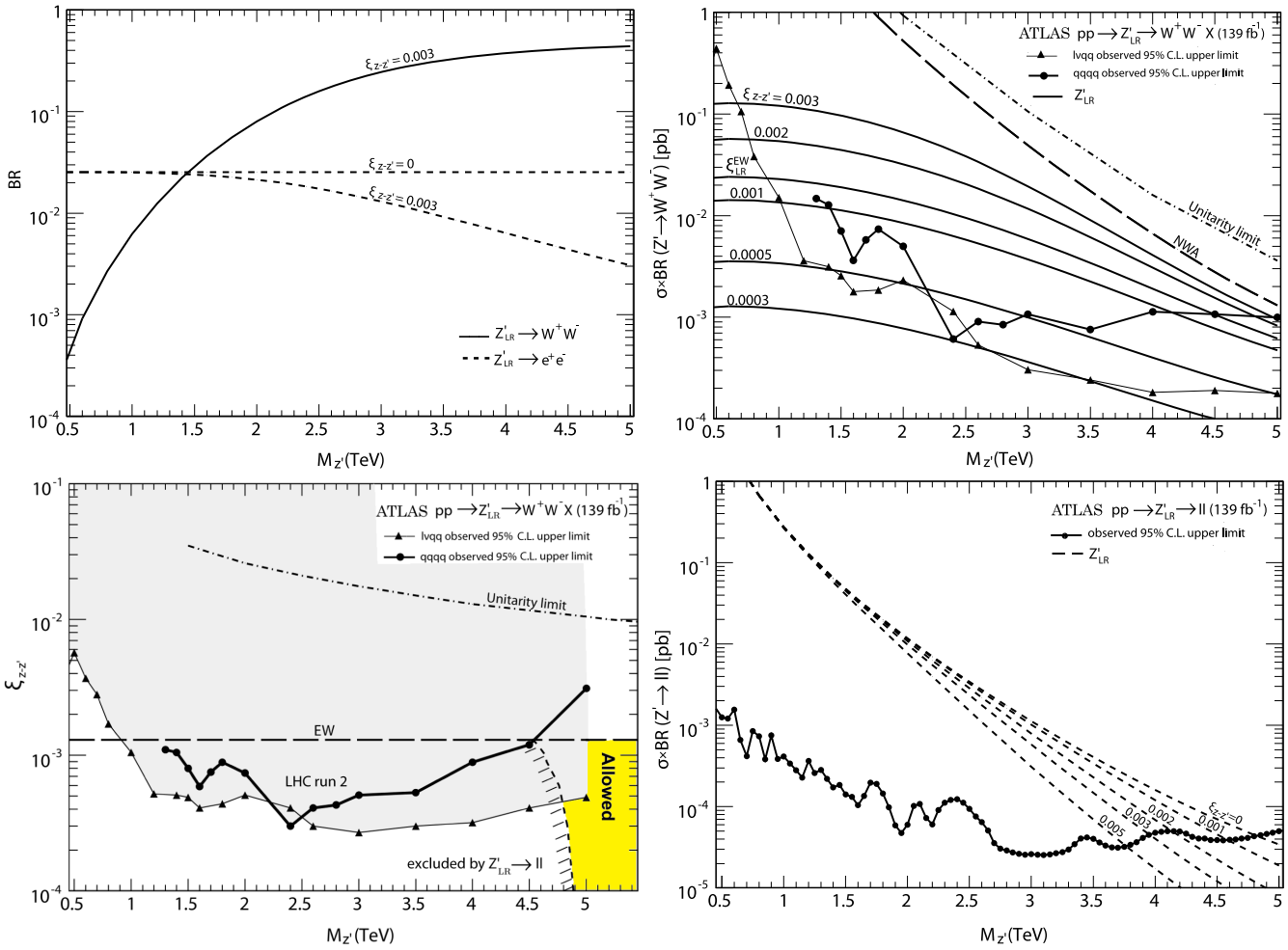

FIG. 8. The Z'_{LR} model. Top-left, top-right, bottom-left, and bottom-right panels: analogous to Figs. 2, 3, 4, and 5, respectively.

[43] with the full run 2 dataset with a time-integrated luminosity of 139 fb^{-1} as well as, for the sake of comparison, in the fully hadronic ($qqqq$) final states [41].

In Fig. 10 (right panel), we show the observed 95% C.L. upper limits on the production cross section times the branching fraction, $\sigma_{95\%} \times \mathrm{BR}(W' \to WZ)$, as a function of the W' mass.

Then, for W' we compute the LHC theoretical production cross section multiplied by the branching ratio into WZ bosons, $\sigma(pp \to W'X) \times \mathrm{BR}(W' \to WZ)$, as a function of the two parameters ($M_{W'}$, $\xi_{W\text{-}W'}$) [38], and compare it with the limits established by the ATLAS experiment, $\sigma_{95\%} \times \mathrm{BR}(W' \to WZ)$. The simulation of signals for the EGM W' is based on a suitably adapted version of the leading-order PYTHIA8.2 event generator [54]. A mass-dependent K factor is adopted to rescale the LO PYTHIA prediction to the NNLO one, using the ZWPROD [64] software. The result is presented as solid curves in the right panel for a mixing factor $\xi_{W\text{-}W'}$ ranging from 10^{-2} down to 3×10^{-4}. The factorization and renormalization scales are both set to the W' mass.

The area below the long-dashed curve labeled "NWA" corresponds to the region where the W' resonance width is predicted to be less than 5% of its mass, corresponding to the best detector resolution of the searches, where the narrow-width assumption is satisfied. We also show a curve labeled "unitarity limit" that corresponds to the unitarity bound (see, e.g., [60] and references therein). It was shown that the saturation of unitarity in the elastic scattering $W^{\pm}Z \to W^{\pm}Z$ leads to the constraint $(g_{W'WZ})_{\max} = g_{WWZ} \cdot M_Z^2/(\sqrt{3} M_{W'} M_W)$ that was adopted in plotting this bound. The constraint was obtained under the assumption that the couplings of the W' to quarks and to gauge bosons have the same Lorentz structure as those of the SM but with rescaled strength.

The theoretical curves for the cross sections $\sigma(pp \to W'X) \times \mathrm{BR}(W' \to WZ)$, in descending order, correspond to values of the W-W' mixing factor $\xi_{W\text{-}W'}$ from 0.01 to 0.0003. The intersection points of the measured upper limits on the production cross section with these theoretical cross sections for various values of

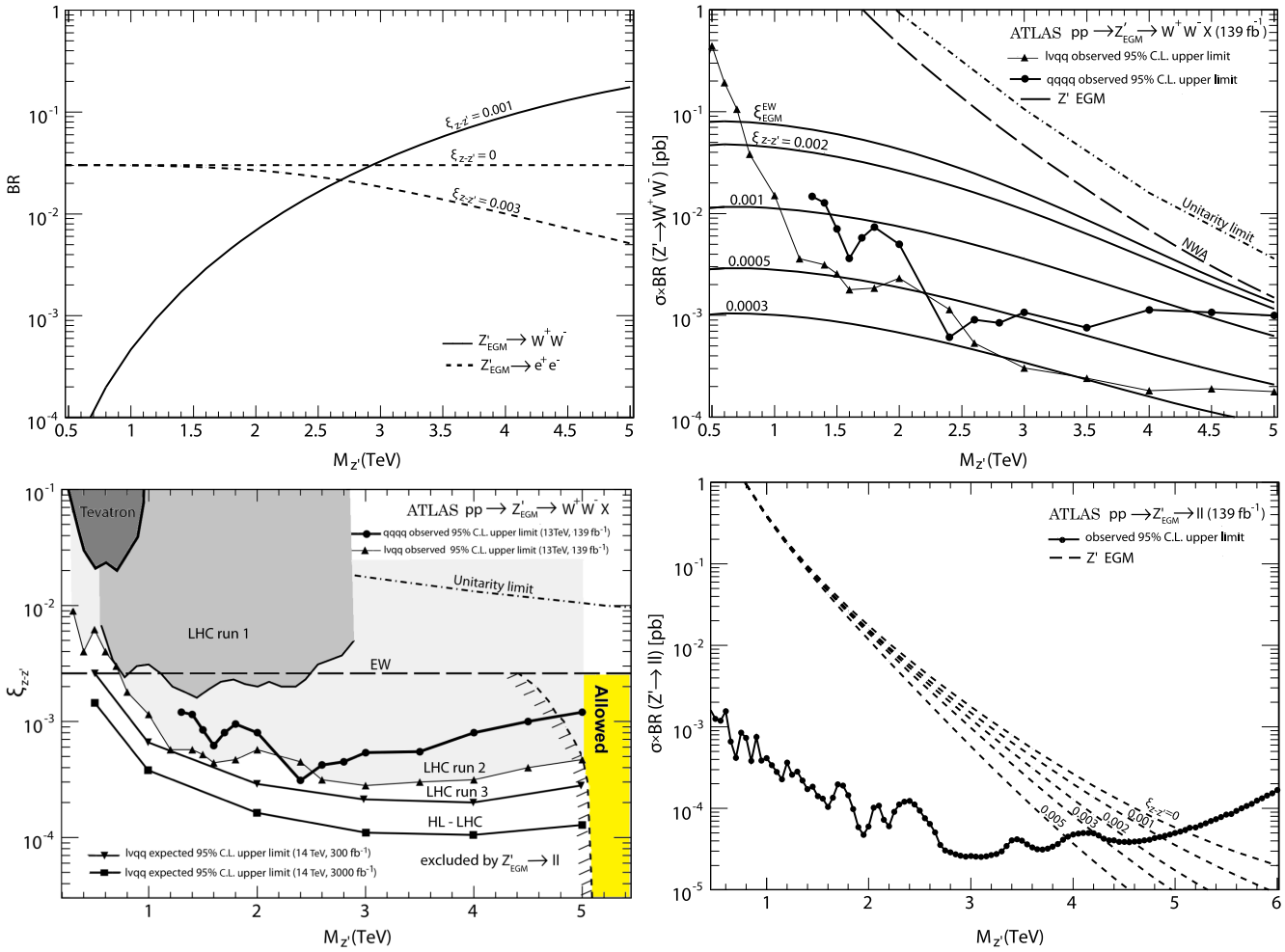

FIG. 9. The Z'_{EGM} model. Top-left, top-right, bottom-left, and bottom-right panels: analogous to Figs. 2, 3, 4, and 5, respectively. Bottom-left panel: Also shown are exclusion regions obtained after incorporating direct search constraints from the CDF and D0 Collaborations which are referred to as Tevatron (the dark shaded area) in $p\bar{p} \to W^+W^-X$ as well as those derived from the LHC measurement of $pp \to WWX$ in run 1 (the gray area) [45]. For comparison, we also show the expected exclusion from run 3 (300 fb^{-1}) and the HL-LHC option (3000 fb^{-1}); see the text.

TABLE II. Observed 95% C.L. lower mass limits on $M_{Z'}$ for different Z' gauge models from $pp \to Z' \to \ell\ell X$ taking into account the effect of potential Z-Z' mixing.

Model	Mixing parameter	$M_{Z'}$ (TeV) lower limits
Z'_ψ	No mixing	4.5
	$\xi^{\mathrm{EW}}_{Z\text{-}Z'} = 1.8 \times 10^{-3}$	3.8
Z'_η	No mixing	4.6
	$\xi^{\mathrm{EW}}_{Z\text{-}Z'} = 4.7 \times 10^{-3}$	3.3
Z'_χ	No mixing	4.8
	$\xi^{\mathrm{EW}}_{Z\text{-}Z'} = 1.6 \times 10^{-3}$	4.2
Z'_{LR}	No mixing	4.9
	$\xi^{\mathrm{EW}}_{Z\text{-}Z'} = 1.3 \times 10^{-3}$	4.5
Z'_{EGM}	No mixing	5.1
	$\xi^{\mathrm{EW}}_{Z\text{-}Z'} = 2.6 \times 10^{-3}$	4.4

$\xi_{W\text{-}W'}$ give the corresponding lower bounds on ($M_{W'}$, $\xi_{W\text{-}W'}$), displayed in Fig. 11, left panel.

Comparison of sensitivities of the process (4) to W' with different decay channels, e.g., $VV \to \ell\nu qq$ and $qqqq$, can be performed by the matching of 95% C.L. upper limits on the production cross section times the branching fraction, $\sigma_{95\%} \times \mathrm{BR}(W' \to WZ)$, which includes the SM branching fractions of the electroweak bosons to the final states in the analysis channel and effects from detector acceptance, as well as reconstruction and selection efficiencies. ATLAS bounds were included according to the Durham HepData repository [42,44].

From a comparison of the upper limits on the production cross section times the branching fraction for semileptonic vs fully hadronic decay channels, one can conclude that the sensitivity of the semileptonic channel dominates over the fully hadronic one within the whole range of the W' mass,

TABLE III. Upper limits on mixing parameters $\xi_{Z\text{-}Z'}$ and $\xi_{W\text{-}W'}$ at 95% C.L. in different models, processes, and experiments (past, Tevatron; present, EW and LHC; future, ILC). We also compare with the expected ILC reach.

Collider, process	$\xi^{\psi}_{Z\text{-}Z'}$	$\xi^{\eta}_{Z\text{-}Z'}$	$\xi^{\chi}_{Z\text{-}Z'}$	$\xi^{\mathrm{LR}}_{Z\text{-}Z'}$	$\xi^{\mathrm{EGM}}_{Z\text{-}Z'}$	$\xi^{\mathrm{EGM}}_{W\text{-}W'}$	$@M'_V$ (TeV)
Tevatron, $p\bar{p} \to Z'/W' \to WW/WZ(\to \ell\nu qq)$ [34]	⋯	⋯	⋯	⋯	2×10^{-2}	2×10^{-2}	0.4–0.9
EW data [1,15]	1.8×10^{-3}	4.7×10^{-3}	1.6×10^{-3}	1.3×10^{-3}	2.6×10^{-3}	$\sim 10^{-2}$	⋯
LHC@13 TeV, 139 fb^{-1}: run 2 (this work)							
$pp \to Z'/W' \to WW/WZ(\to qqqq)$	2.9×10^{-4}	2.7×10^{-4}	3.8×10^{-4}	3.0×10^{-4}	3.1×10^{-4}	4.3×10^{-4}	1.3–5.0
$pp \to Z' \to WW(\to \ell\nu\, qq)$	2.5×10^{-4}	2.4×10^{-4}	3.3×10^{-4}	2.7×10^{-4}	2.8×10^{-4}	⋯	0.5–5.0
$pp \to W' \to WZ(\to \ell\nu/\ell\ell/\nu\nu\, qq)$	⋯	⋯	⋯	⋯	⋯	2.9×10^{-4}	0.5–5.0
ILC@0.5 TeV, 0.5 ab^{-1}, $e^+e^- \to W^+W^-$ [63]	2.3×10^{-3}	1.6×10^{-3}	1.5×10^{-3}	1.4×10^{-3}	1.2×10^{-3}	⋯	≥ 3
ILC@1.0 TeV, 1.0 ab^{-1}, $e^+e^- \to W^+W^-$ [63]	0.6×10^{-3}	0.5×10^{-3}	0.4×10^{-3}	0.4×10^{-3}	0.3×10^{-3}	⋯	≥ 3

from 0.5 to 5 TeV. These features are illustrated in Figs. 10 (right panel) and 11 (left panel).

For reference, we display limits on the W' parameters from the Tevatron (CDF and D0) as well as from ATLAS and CMS obtained at 7 and 8 TeV of LHC data taking in run 1 denoted "LHC run 1" [38]. Figure 11 (left panel) shows that the experiments CDF and D0 at the Tevatron exclude EGM W' bosons with $\xi_{W\text{-}W'} \gtrsim 2 \times 10^{-2}$ in the resonance mass range 0.25 TeV $< M_{W'} <$ 1 TeV at the 95% C.L., whereas the LHC in run 1 improved those constraints, excluding W' boson parameters at $\xi_{W\text{-}W'} \gtrsim 2 \times 10^{-3}$ in the mass range 0.2 TeV $< M_{W'} <$ 2 TeV.

As expected, the increase of the time-integrated luminosity up to 139 fb^{-1} leads to dominant sensitivity of the semileptonic channel over the whole resonance mass range of 0.5 TeV $< M_{W'} <$ 5 TeV, and it allows one to set stronger constraints on the mixing angle $\xi_{W\text{-}W'}$, excluding $\xi_{W\text{-}W'} > 2.3 \times 10^{-4}$ as shown in Fig. 11. Our results extend the sensitivity beyond the corresponding CDF Tevatron results [34] as well as the ATLAS and CMS sensitivity attained at 7 and 8 TeV. Also, for the first time, we set W' limits as functions of the mass $M_{W'}$ and mixing factor $\xi_{W\text{-}W'}$ from the study of the diboson production and subsequent decay into semileptonic final states at the LHC at 13 TeV with the full ATLAS run 2 dataset. The exclusion region obtained in this way on the parameter space of the W' naturally supersedes the corresponding exclusion area obtained for a time-integrated luminosity of 36.1 fb^{-1} in the semileptonic channel as reported in Ref. [38]. The limits on the W' parameters presented in this section obtained from the diboson WZ production in semileptonic final states, corresponding to a time-integrated luminosity of 139 fb^{-1}, are the best to date.

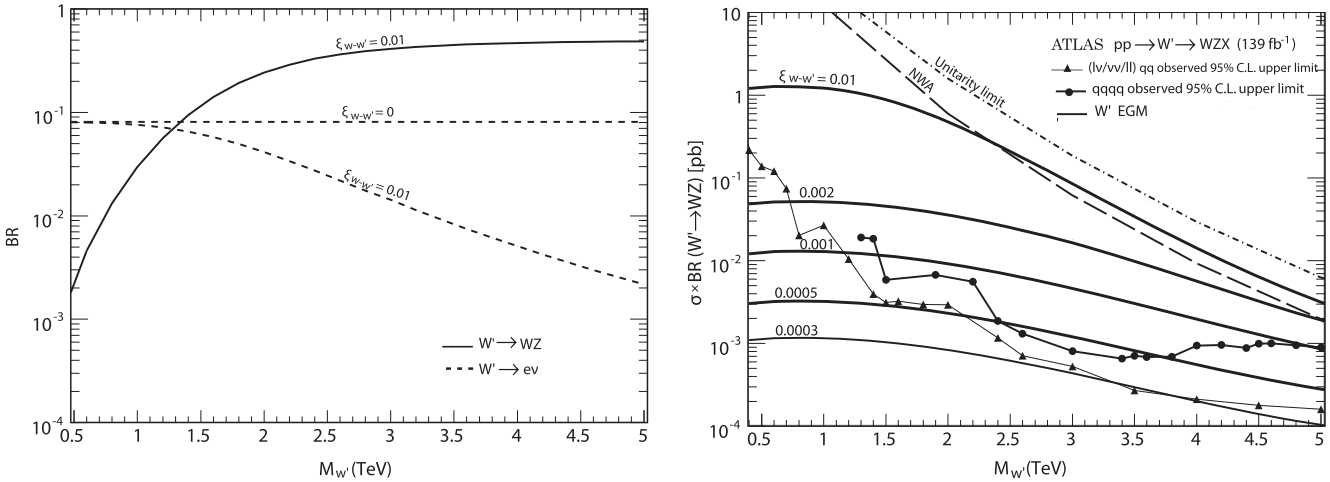

FIG. 10. Left panel: branching ratio BR($W' \to WZ$) (solid line) vs $M_{W'}$ in the EGM for W-W' mixing factor $\xi_{W\text{-}W'} = 10^{-2}$. Dashed line: BR($W' \to e\nu$) for $\xi_{W\text{-}W'} = 0$ (W'_{SSM}) and $\xi_{W\text{-}W'} = 0.01$. Right panel: 95% C.L. upper limits on $\sigma_{95\%} \times \mathrm{BR}(W' \to WZ)$, showing ATLAS data on the fully hadronic and semileptonic final states for 139 fb^{-1} [41,43]. The theoretical production cross sections $\sigma(pp \to W'X) \times \mathrm{BR}(W' \to WZ)$ for the EGM are calculated from PYTHIA with a W' mass-dependent K factor, given by solid curves, for mixing factor $\xi_{W\text{-}W'}$ ranging from 10^{-2} down to 3×10^{-4}. The NWA and unitarity constraints are also shown [38,60].

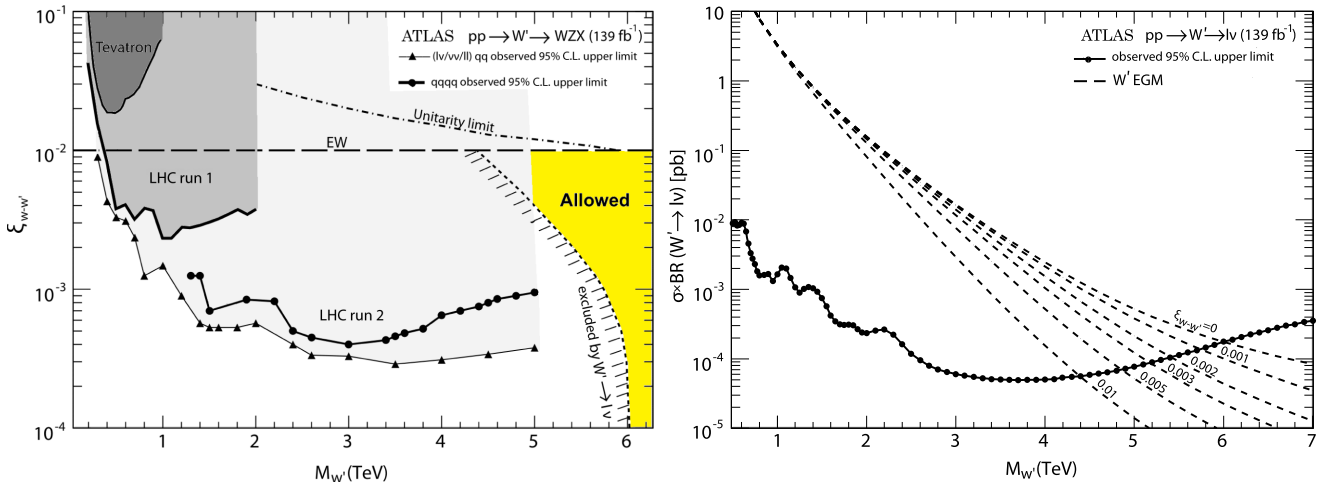

FIG. 11. Left panel: 95% C.L. exclusion regions in the two-dimensional ($M_{W'}$, $\xi_{W\text{-}W'}$) plane obtained from the precision electroweak data (horizontal dashed straight line labeled "EW") and direct search constraints from the Tevatron in $p\bar{p} \to WZX$ (dark shaded area) as well as from the LHC searches for $pp \to WZX$ at 7 and 8 TeV (run 1) (gray area) and at 13 TeV from diboson $W' \to WZ$ production in hadronic and semileptonic final states using the full run 2 ATLAS dataset. The region above each curve for the WZ channel is excluded. The steep curve labeled "excluded by $W' \to \ell\nu$" shows the exclusion based on the dilepton channel $pp \to \ell\nu X$. The overall allowed region for the EGM W' boson is shown as the yellow area. Right panel: solid line: observed 95% C.L. upper bound on the W' production cross section times branching ratio to two leptons, $\sigma_{95\%} \times \mathrm{BR}(W' \to \ell\nu)$, obtained in the combined channels (electron and muon) at the LHC with integrated luminosity $\mathcal{L}_{\mathrm{int}} = 139$ fb^{-1} by the ATLAS Collaboration [7]. Dashed lines: theoretical production cross section $\sigma(pp \to W') \times \mathrm{BR}(W' \to \ell\nu)$ for the EGM W' boson, calculated from PYTHIA8.2 with an NNLO K factor. These curves, in descending order, correspond to values of the W-W' mixing factor ξ from 0 to 0.01.

D. W-W' mixing effects in dilepton decay of $W' \to \ell\nu$

The above analysis was for the diboson process (4), employing one of the most recent ATLAS searches [41,43]. Next, we turn to the dilepton production process (2); this process gives valuable complementary information. Unlike the SSM, where there is no W-W' mixing, in the EGM we consider a nonzero mixing $\xi_{W\text{-}W'}$ in the analysis of the $W' \to \ell\nu$ process. As described in Sec. IV B, this results in a modification of $\mathrm{BR}(W' \to e\nu)$.

We compute the W' production cross section at LO with PYTHIA8.2 [54], $\sigma(pp \to W')$, multiplied by the branching ratio into two leptons, $\ell\nu$ (here $\ell = e$), i.e., $\sigma(pp \to W') \times \mathrm{BR}(W' \to e\nu)$, as a function of $M_{W'}$. A mass-dependent K factor is applied, based on NNLO QCD cross sections as calculated with FEWZ3.1 [65,66]. The K factor varies approximately from 1.3 to 1.1 for the range of W' masses studied in this analysis, namely, from 0.5 to 6.0 TeV. The NNLO corrections decrease with increasing W' mass up to around 4.5 TeV [67]. For higher W' masses, the K factor increases again and becomes similar to the low-mass values.

The product of the NNLO W' theoretical production cross section and branching fraction, $\sigma(pp \to W') \times \mathrm{BR}(W' \to e\nu)$, for the W' boson for EGM strongly depends on the W' mass and is given by dashed curves, in descending order, corresponding to values of the mixing factor ξ from 0.0 to 0.01, as displayed in Fig. 11 (right panel).

Comparison of $\sigma(pp \to W') \times \mathrm{BR}(W' \to e\nu)$ vs $\sigma_{95\%} \times \mathrm{BR}(W' \to \ell\nu)$ displayed in Fig. 11 (right panel) allows us to read off an allowed mixing for a given mass value; higher masses are allowed for smaller mixing, for the reason stated above. That comparison can be translated into constraints on the two-dimensional $M_{W'} - \xi_{W\text{-}W'}$ parameter plane, as shown in Fig. 11 (left panel).

The above results are based on data corresponding to an integrated luminosity of 139 fb^{-1} taken by the ATLAS Collaboration at $\sqrt{s} = 13$ TeV in run 2 [7]. The corresponding lower limits on the W' boson mass of 6 TeV (at $\xi_{W\text{-}W'} = 0$) were set at 95% C.L. from combination of the electron and muon channels. Notice that, similar to the case of Z' bosons, at $\xi^{\mathrm{EW}}_{W\text{-}W'} = 10^{-2}$ these limits become weaker, reaching ~4.4 TeV, as illustrated in Fig. 11 (left and right panels).

V. CONCLUDING REMARKS

Examination of the diboson, WW and WZ, and dilepton, $\ell\ell$ and $\ell\nu$, production at the LHC with the 13 TeV dataset allows us to place stringent constraints on the Z-Z' and W-W' mixing parameters as well as on the Z' and W' masses for benchmark extended models, respectively. We derived such limits by using the full ATLAS run 2 dataset recorded at the CERN LHC, with integrated luminosity of 139 fb^{-1}. The constraints are summarized in Table III. We note that, in a situation when the limit is dominated by

statistical errors, the K factor plays a role similar to integrated luminosity. Thus, if we had adopted the same K factor for the WW (WZ) channel as for the dilepton channel, the bounds on ξ would have been slightly weaker, by a factor $K^{1/4} \simeq 1.17$ for the Z' case [37].

By comparing the experimental limits to the theoretical predictions for the total cross section of the Z' and W' resonant production and their subsequent decays into WW or WZ pairs, we show that the derived constraints on the mixing parameters, $\xi_{Z\text{-}Z'}$ and $\xi_{W\text{-}W'}$, are substantially improved with respect to those obtained from the global analysis of low-energy electroweak data, as well as compared to the diboson production study performed at the Tevatron, and to those published previously and based on the LHC run 1 as well as at 13 TeV in run 2 at a time-integrated luminosity of $\sim$36 fb^{-1} and are the most stringent bounds to date. Further constraining of this mixing can be achieved from the analysis of data to be collected in run 3 as well as at the next options of hadron colliders such as HL-LHC and HE-LHC [61,68].

ACKNOWLEDGMENTS

It is a pleasure to thank Dr. Anurag Tripathi for discussions on K factors. This research has been partially supported by the Abdus Salam ICTP (TRIL Program) and by the Belarusian Republican Foundation for Fundamental Research, F20MC-004 and F20MC-005. The work of P. O. has been supported by the Research Council of Norway.

[1] P. A. Zyla *et al.* (Particle Data Group), Review of particle physics, Prog. Theor. Exp. Phys. **2020**, 083C01 (2020).
[2] G. Aad *et al.* (ATLAS Collaboration), Search for high-mass dilepton resonances using 139 fb^{-1} of pp collision data collected at $\sqrt{s} = 13$ TeV with the ATLAS detector, Phys. Lett. B **796**, 68 (2019).
[3] Durham HepData repository, https://www.hepdata.net/record/ins1725190 (2020).
[4] CMS Collaboration, Search for a narrow resonance in high-mass dilepton final states in proton-proton collisions using 140 fb^{-1} of data at $\sqrt{s} = 13$ TeV, CERN Report No. CMS-PAS-EXO-19-019, 2019, https://cds.cern.ch/record/2684757.
[5] A. Zucchetta (ATLAS and CMS Collaborations), Heavy resonances (W', Z', jets) in ATLAS and CMS in Run 2, in *Proceedings of the 54th Rencontres de Moriond on Electroweak Interactions and Unified Theories* (2019), pp. 85–90 [arXiv:1905.06607].
[6] CMS Collaboration, Search for high mass resonances in dielectron final state, CERN Report No. CMS-PAS-EXO-18-006, 2018, https://cds.cern.ch/record/2308270?ln=en.
[7] G. Aad *et al.* (ATLAS Collaboration), Search for a heavy charged boson in events with a charged lepton and missing transverse momentum from pp collisions at $\sqrt{s} = 13$ TeV with the ATLAS detector, Phys. Rev. D **100**, 052013 (2019).
[8] G. Altarelli, B. Mele, and M. Ruiz-Altaba, Searching for new heavy vector bosons in $p\bar{p}$ colliders, Z. Phys. C **45**, 109 (1989); Erratum, Z. Phys. C **47**, 676 (1990).
[9] M. Schmaltz and C. Spethmann, Two simple W' models for the early LHC, J. High Energy Phys. 07 (2011) 046.
[10] C. Grojean, E. Salvioni, and R. Torre, A weakly constrained W' at the early LHC, J. High Energy Phys. 07 (2011) 002.
[11] T. Jezo, M. Klasen, and I. Schienbein, LHC phenomenology of general $SU(2) \times SU(2) \times U(1)$ models, Phys. Rev. D **86**, 035005 (2012).
[12] Q.-H. Cao, Z. Li, J.-H. Yu, and C. P. Yuan, Discovery and identification of W' and Z' in $SU(2) \times SU(2) \times U(1)$ models at the LHC, Phys. Rev. D **86**, 095010 (2012).
[13] B. A. Dobrescu and Z. Liu, Heavy Higgs bosons and the 2 TeV W' boson, J. High Energy Phys. 10 (2015) 118.
[14] P. Langacker, The physics of heavy Z' gauge bosons, Rev. Mod. Phys. **81**, 1199 (2009).
[15] J. Erler, P. Langacker, S. Munir, and E. Rojas, Improved constraints on Z-prime bosons from electroweak precision data, J. High Energy Phys. 08 (2009) 017.
[16] J. L. Hewett and T. G. Rizzo, Low-energy phenomenology of superstring inspired E(6) models, Phys. Rep. **183**, 193 (1989).
[17] A. Leike, The phenomenology of extra neutral gauge bosons, Phys. Rep. **317**, 143 (1999).
[18] M. Dittmar, A.-S. Nicollerat, and A. Djouadi, Z-prime studies at the LHC: An update, Phys. Lett. B **583**, 111 (2004).
[19] P. Osland, A. A. Pankov, A. V. Tsytrinov, and N. Paver, Spin and model identification of Z' bosons at the LHC, Phys. Rev. D **79**, 115021 (2009).
[20] S. Godfrey and T. Martin, Z' discovery reach at future hadron colliders: A Snowmass white paper, in *Proceedings of Community Summer Study 2013: Snowmass on the Mississippi*(2013) [arXiv:1309.1688].
[21] V. V. Andreev, P. Osland, and A. A. Pankov, Precise determination of Z-Z' mixing at the CERN LHC, Phys. Rev. D **90**, 055025 (2014).
[22] A. V. Gulov, A. A. Pankov, A. O. Pevzner, and V. V. Skalozub, Model-independent constraints on the Abelian Z' couplings within the ATLAS data on the dilepton production processes at $\sqrt{s} = 13$ TeV, Nonlinear Phenom. Complex Syst. **21**, 21 (2018), https://old.inspirehep.net/record/1663295.
[23] T. Bandyopadhyay, G. Bhattacharyya, D. Das, and A. Raychaudhuri, Reappraisal of constraints on Z' models from unitarity and direct searches at the LHC, Phys. Rev. D **98**, 035027 (2018).
[24] T. Bandyopadhyay, D. Das, R. Pasechnik, and J. Rathsman, Complementary bound on the W' mass from Higgs boson to diphoton decays, Phys. Rev. D **99**, 115021 (2019).

[25] E. Eichten, I. Hinchliffe, K. D. Lane, and C. Quigg, Super collider physics, Rev. Mod. Phys. **56**, 579 (1984); Erratum, Rev. Mod. Phys. **58**, A1065 (1986).

[26] L. Randall and R. Sundrum, A Large Mass Hierarchy from a Small Extra Dimension, Phys. Rev. Lett. **83**, 3370 (1999).

[27] H. Davoudiasl, J. L. Hewett, and T. G. Rizzo, Experimental probes of localized gravity: On and off the wall, Phys. Rev. D **63**, 075004 (2001).

[28] K. Lane and S. Mrenna, The collider phenomenology of technihadrons in the technicolor straw Man model, Phys. Rev. D **67**, 115011 (2003).

[29] E. Eichten and K. Lane, Low-scale technicolor at the Tevatron and LHC, Phys. Lett. B **669**, 235 (2008).

[30] K. Agashe, R. Contino, and A. Pomarol, The Minimal composite Higgs model, Nucl. Phys. **B719**, 165 (2005).

[31] G. F. Giudice, C. Grojean, A. Pomarol, and R. Rattazzi, The strongly-interacting light Higgs, J. High Energy Phys. 06 (2007) 045.

[32] D. Pappadopulo, A. Thamm, R. Torre, and A. Wulzer, Heavy vector triplets: Bridging theory and data, J. High Energy Phys. 09 (2014) 060.

[33] H.-J. He, Yu.-P. Kuang, Y.-H. Qi, B. Zhang, A. Belyaev, R. S. Chivukula, N. D. Christensen, A. Pukhov, and E. H. Simmons, CERN LHC signatures of new gauge bosons in minimal Higgsless model, Phys. Rev. D **78**, 031701 (2008).

[34] T. Aaltonen *et al.* (CDF Collaboration), Search for WW and WZ Resonances Decaying to Electron, Missing E_T, and Two Jets in $p\bar{p}$ Collisions at $\sqrt{s} = 1.96$ TeV, Phys. Rev. Lett. **104**, 241801 (2010).

[35] S. Schael *et al.* (ALEPH, DELPHI, L3, OPAL, SLD, LEP Electroweak Working Group, SLD Electroweak Group, SLD Heavy Flavour Group), Precision electroweak measurements on the Z resonance, Phys. Rep. **427**, 257 (2006).

[36] P. Osland, A. A. Pankov, and A. V. Tsytrinov, Probing Z-Z' mixing with ATLAS and CMS resonant diboson production data at the LHC at $\sqrt{s} = 13$ TeV, Phys. Rev. D **96**, 055040 (2017).

[37] I. D. Bobovnikov, P. Osland, and A. A. Pankov, Improved constraints on the mixing and mass of Z' bosons from resonant diboson searches at the LHC at $\sqrt{s} = 13$ TeV and predictions for Run II, Phys. Rev. D **98**, 095029 (2018).

[38] I. A. Serenkova, P. Osland, and A. A. Pankov, Improved bounds on W-W' mixing with ATLAS resonant WZ production data at the LHC at $\sqrt{s} = 13$ TeV, Phys. Rev. D **100**, 015007 (2019).

[39] M. Aaboud *et al.* (ATLAS Collaboration), Search for WW/WZ resonance production in $\ell\nu qq$ final states in pp collisions at $\sqrt{s} = 13$ TeV with the ATLAS detector, J. High Energy Phys. 03 (2018) 042.

[40] A. M. Sirunyan *et al.* (CMS Collaboration), Search for massive resonances decaying into WW, WZ, ZZ, qW, and qZ with dijet final states at $\sqrt{s} = 13$ TeV, Phys. Rev. D **97**, 072006 (2018).

[41] G. Aad *et al.* (ATLAS Collaboration), Search for diboson resonances in hadronic final states in 139 fb^{-1} of pp collisions at $\sqrt{s} = 13$ TeV with the ATLAS detector, J. High Energy Phys. 09 (2019) 091; Erratum, J. High Energy Phys. 06 (2020) 42.

[42] Durham HepData repository, https://www.hepdata.net/record/ins1740685 (2020).

[43] G. Aad *et al.* (ATLAS Collaboration), Search for heavy diboson resonances in semileptonic final states in pp collisions at $\sqrt{s} = 13$ TeV with the ATLAS detector, Eur. Phys. J. C **80**, 1165 (2020).

[44] Durham HepData repository, https://www.hepdata.net/record/ins1793572 (2020).

[45] A. A. Pankov, P. Osland, I. A. Serenkova, and V. A. Bednyakov, High-precision limits on W-W' and Z-Z' mixing from diboson production using the full LHC Run 2 ATLAS data set, Eur. Phys. J. C **80**, 503 (2020).

[46] M. Aaboud *et al.* (ATLAS Collaboration), Searches for heavy diboson resonances in pp collisions at $\sqrt{s} = 13$ TeV with the ATLAS detector, J. High Energy Phys. 09 (2016) 173.

[47] A. M. Sirunyan *et al.* (CMS Collaboration), Combination of searches for heavy resonances decaying to WW, WZ, ZZ, WH, and ZH boson pairs in proton–proton collisions at $\sqrt{s} = 8$ and 13 TeV, Phys. Lett. B **774**, 533 (2017).

[48] E. Salvioni, G. Villadoro, and F. Zwirner, Minimal Z-prime models: Present bounds and early LHC reach, J. High Energy Phys. 11 (2009) 068.

[49] J. Kang and P. Langacker, Z' discovery limits for supersymmetric E(6) models, Phys. Rev. D **71**, 035014 (2005).

[50] M. S. Chanowitz and M. K. Gaillard, The TeV physics of strongly interacting W's and Z's, Nucl. Phys. **B261**, 379 (1985).

[51] V. D. Barger and K. Whisnant, Heavy Z boson decays to two bosons in $E(6)$ superstring models, Phys. Rev. D **36**, 3429 (1987).

[52] V. Barger, P. Langacker, and H.-S. Lee, Six-Lepton Z-Prime Resonance at the LHC, Phys. Rev. Lett. **103**, 251802 (2009).

[53] C. Dib and F. J. Gilman, Extra neutral gauge bosons in electron-positron collisions at resonance, Phys. Rev. D **36**, 1337 (1987).

[54] T. Sjöstrand, S. Ask, J. R. Christiansen, R. Corke, N. Desai, P. Ilten, S. Mrenna, S. Prestel, C. O. Rasmussen, and P. Z. Skands, An introduction to PYTHIA8.2, Comput. Phys. Commun. **191**, 159 (2015).

[55] S. Frixione, A next-to-leading order calculation of the cross-section for the production of W^+W^- pairs in hadronic collisions, Nucl. Phys. **B410**, 280 (1993).

[56] N. Agarwal, V. Ravindran, V. K. Tiwari, and A. Tripathi, Next-to-leading order QCD corrections to W^+W^- production at the LHC in Randall Sundrum model, Phys. Lett. B **690**, 390 (2010).

[57] T. Gehrmann, M. Grazzini, S. Kallweit, P. Maierhöfer, A. von Manteuffel, S. Pozzorini, D. Rathlev, and L. Tancredi, W^+W^- Production at Hadron Colliders in Next to Next to Leading Order QCD, Phys. Rev. Lett. **113**, 212001 (2014).

[58] M. Aaboud *et al.* (ATLAS Collaboration), Search for new high-mass phenomena in the dilepton final state using 36 fb^{-1} of proton-proton collision data at $\sqrt{s} = 13$ TeV with the ATLAS detector, J. High Energy Phys. 10 (2017) 182.

[59] A. M. Sirunyan *et al.* (CMS Collaboration), Search for high-mass resonances in dilepton final states in proton-proton collisions at $\sqrt{s} = 13$ TeV, J. High Energy Phys. 06 (2018) 120.

[60] A. Alves, O. J. P. Eboli, D. Goncalves, M. C. Gonzalez-Garcia, and J. K. Mizukoshi, Signals for new spin-1 resonances in electroweak gauge boson pair production at the LHC, Phys. Rev. D **80**, 073011 (2009).

[61] X. C. Vidal *et al.*, Report from Working Group 3: Beyond the Standard Model physics at the HL-LHC and HE-LHC, CERN Yellow Rep. Monogr. **7**, 585 (2019).

[62] The ATLAS Collaboration, Prospects for searches for heavy Z' and W' bosons in fermionic final states with the ATLAS experiment at the HL-LHC (2018).

[63] V. V. Andreev, G. Moortgat-Pick, P. Osland, A. A. Pankov, and N. Paver, Discriminating Z' from anomalous trilinear gauge coupling signatures in $e^+e^- \to W^+W^-$ at ILC with polarized beams, Eur. Phys. J. C **72**, 2147 (2012).

[64] R. Hamberg, W. L. van Neerven, and T. Matsuura, A complete calculation of the order α_s^2 correction to the Drell-Yan K factor, Nucl. Phys. **B359**, 343 (1991); Erratum, Nucl. Phys. **B644**, 403 (2002).

[65] R. Gavin, Y. Li, F. Petriello, and S. Quackenbush, FEWZ2.0: A code for hadronic Z production at next-to-next-to-leading order, Comput. Phys. Commun. **182**, 2388 (2011).

[66] Y. Li and F. Petriello, Combining QCD and electroweak corrections to dilepton production in FEWZ, Phys. Rev. D **86**, 094034 (2012).

[67] V. Khachatryan *et al.* (CMS Collaboration), Search for heavy gauge W' boson in events with an energetic lepton and large missing transverse momentum at $\sqrt{s} = 13$ TeV, Phys. Lett. B **770**, 278 (2017).

[68] A. Abada *et al.* (FCC Collaboration), HE-LHC: The high-energy large hadron collider: Future circular collider conceptual design report Volume 4, Eur. Phys. J. Special Topics **228**, 1109 (2019).